

# The Genesis of Molecular Volcano Plots

Published as part of the Accounts of Chemical Research special issue "Data Science Meets Chemistry".

Matthew D. Wodrich, Boodsarin Sawatlon, Michael Busch, and Clemence Corminboeuf\*



Cite This: *Acc. Chem. Res.* 2021, 54, 1107–1117



Read Online

ACCESS |

Metrics & More

Article Recommendations

**CONSPECTUS:** For the past two decades, linear free energy scaling relationships and volcano plots have seen frequent use as computational tools that aid in understanding and predicting the catalytic behavior of heterogeneous and electrocatalysts. Based on Sabatier's principle, which states that a catalyst should bind a substrate neither too strongly nor too weakly, volcano plots provide an estimate of catalytic performance (*e.g.*, overpotential, catalytic cycle thermodynamics/kinetics, *etc.*) through knowledge of a descriptor variable. By the use of linear free energy scaling relationships, the value of this descriptor is employed to estimate the relative energies of other catalytic cycle intermediates/transition states. Postprocessing of these relationships leads to a volcano curve that reveals the anticipated performance of each catalyst, with the best species appearing on or near the peak or plateau. While the origin of volcanoes is undoubtedly rooted in examining heterogeneously catalyzed reactions, only recently has this concept been transferred to the realm of homogeneous catalysis. This Account summarizes the work done by our group in implementing and refining "molecular volcano plots" for use in analyzing and predicting the behavior of homogeneous catalysts.

We begin by taking the reader through the initial proof-of-principle study that transferred the model from heterogeneous to homogeneous catalysis by examining thermodynamic aspects of a Suzuki–Miyaura cross-coupling reaction. By establishing linear free energy scaling relationships and reproducing the volcano shape, we definitively showed that volcano plots are also valid for homogeneous systems. On the basis of this key finding, we further illustrate how unified pictures of C–C cross-coupling thermodynamics were created using three-dimensional molecular volcanoes.

The second section highlights an important transformation from "thermodynamic" to "kinetic" volcanoes by using the descriptor variable to directly estimate transition state barriers. Taking this idea further, we demonstrate how volcanoes can be used to directly predict an experimental observable, the turnover frequency. Discussion is also provided on how different flavors of molecular volcanoes can be used to analyze aspects of homogeneous catalysis of interest to experimentalists, such as determining the product selectivity and probing the substrate scope.

The third section focuses on incorporating machine learning approaches into molecular volcanoes and invoking big-data-type approaches in the analysis of catalytic behavior. Specifically, we illustrate how machine learning can be used to predict the value of the descriptor variable, which facilitates nearly instantaneous screening of thousands of catalysts. With the large amount of data created from the machine learning/volcano plot tandem, we show how the resulting database can be mined to garner an enhanced understanding of catalytic processes. Emphasis is also placed on the latest generation of augmented volcano plots, which differ fundamentally from earlier volcanoes by elimination of the use of linear free energy scaling relationships and by assessment of the similarity of the complete catalytic cycle energy profile to that for an ideal reference species that is used to discriminate catalytic performance.

We conclude by examining a handful of applications of molecular volcano plots to interesting problems in homogeneous catalysis and offering thoughts on the future prospects and uses of this new set of tools.



## KEY REFERENCES

- Busch, M.; Wodrich, M. D.; Corminboeuf, C. Linear Scaling Relationships and Volcano Plots in Homogeneous Catalysis – Revisiting the Suzuki Reaction. *Chem. Sci.* 2015, 6, 6754–6761. *This is an initial proof-of-principle*

Received: December 17, 2020  
Published: February 11, 2021



study showing that linear scaling relationships and volcano plots can be used to study homogeneous catalysis.

- Meyer, B.; Sawatlon, B.; Heinen, S.; von Lilienfeld, O. A.; Corminboeuf, C. Machine Learning Meets Volcano Plots: Computational Discovery of Cross-Coupling Catalysts. *Chem. Sci.* **2018**, *9*, 7069–7077.<sup>2</sup> This paper describes a protocol for combining machine learning and molecular volcano plots to rapidly screen thousands of prospective catalysts.
- Wodrich, M. D.; Sawatlon, B.; Solel, E.; Kozuch, S.; Corminboeuf, C. Activity-Based Screening of Homogeneous Catalysts through the Rapid Assessment of Theoretically Derived Turnover Frequencies. *ACS Catal.* **2019**, *9*, 5716–5725.<sup>3</sup> This paper presents a method to directly assess and screen homogeneous catalysts using an experimentally measurable quantity of catalytic activity.
- Wodrich, M. D.; Fabrizio, A.; Meyer, B.; Corminboeuf, C. Data-Powered Augmented Volcano Plots for Homogeneous Catalysis. *Chem. Sci.* **2020**, *11*, 12070–12080.<sup>4</sup> This paper presents a new tool to measure and assess the closeness of the energetics for an entire catalytic cycle to that of an ideal reference species.

## INTRODUCTION

Volcano plots are efficient tools for optimizing catalytic reactions and correspondingly have found widespread use within many areas of catalysis. Historically, these plots are derived from Sabatier's principle,<sup>5,6</sup> which states that an ideal catalyst should neither bind the products too strongly nor bind the reactants too weakly. This concept was put into practice in the 1950s independently by Gerischer<sup>7</sup> and Parsons<sup>8</sup> as a means to visualize the activities of metals toward electrochemical H<sub>2</sub> evolution. As in modern volcano plots, those early works utilized a descriptor variable (e.g., the binding energy of hydrogen) plotted along the x axis and a measurement of catalytic activity (e.g., the experimental current density) plotted on the y axis. In line with Sabatier's principle, the resulting volcano shape (see Figure 1) demonstrates a clear relationship between the value of the descriptor variable and catalytic activity. The volcano shape can be subdivided into three regions: the left slope, where catalysts bind intermediates too strongly (*i.e.*, the “strong-binding” side of the volcano); the right slope, where catalysts bind intermediates too weakly (*i.e.*, the “weak-binding” side of the volcano); and finally an ideal binding region on the volcano plateau, where catalysts bind intermediates neither too strongly nor too weakly. Catalysts that fall into this region (*i.e.*, those located at or near the volcano plateau or peak) satisfy Sabatier's principle and are likely to be among the best catalysts for a given reaction.

The appealing simplicity of the volcano concept led to numerous applications in the fields of electrocatalysis<sup>9,10</sup> and heterogeneous catalysis<sup>11–16</sup> over the following decades. Beginning in the early 2000s, theoretical treatments of volcano plots began appearing with increasing frequency, largely as a result of the work by Nørskov. In part, this growth can be ascribed to the rise of density functional theory (DFT) computations that provided direct access to the key energetic quantities needed to construct the plots, specifically the energy of the descriptor intermediate and a measure of activity, such as the thermodynamic overpotential.<sup>17–19</sup> The subsequent realization that linear free energy scaling relationships (LFESRs) govern the relative stabilities of different catalytic cycle

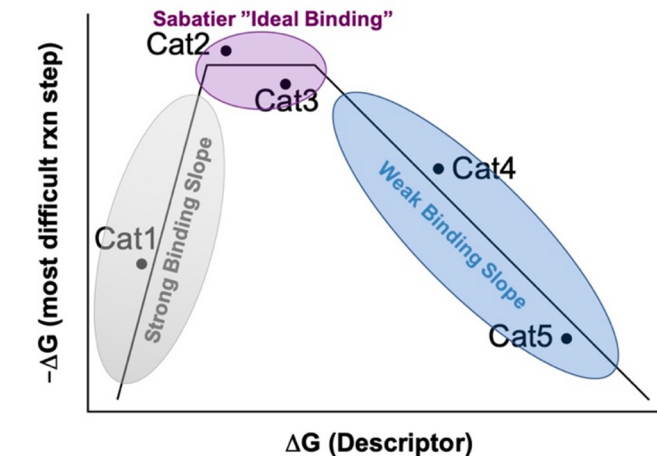


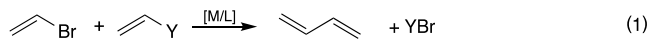
**Figure 1.** Schematic volcano plot. The descriptor value is plotted along the x axis and the negative of the free energy of the most difficult reaction step of the catalytic cycle (or another measure of catalytic activity) along the y axis. Catalysts with the best thermodynamic/kinetic profiles (Cat2 and Cat3) appear near the volcano plateau (or peak) in the Sabatier ideal binding region (purple). Catalysts having overly strong catalyst–substrate interactions (Cat1) appear along the left “strong-binding” slope (gray), while catalysts with overly weak catalyst–substrate interactions (Cat4 and Cat5) appear along the “weak-binding” right slope (blue).

intermediates in the form of binding energies<sup>20,21</sup> as well as transition state barriers<sup>18,22</sup> further provided a route for obtaining the overall volcano shape for any given reaction mechanism through mathematical manipulation of the LFESRs. Correspondingly, the global limitations for many reactions of interest were obtained, as exemplified by Rossmeisl for the water oxidation reaction over transition metal oxides.<sup>23,24</sup> Other more recent advancements include employing volcano plots to examine the stability of materials<sup>25</sup> or account for competing reaction mechanisms.<sup>26,27</sup>

In spite of their simplicity and predictive power, volcano plots and the LFESRs on which they are built have remained nearly exclusively the province of electrocatalysis and heterogeneous catalysis. Although abstractly proposed by Swiegers in 2008,<sup>28</sup> in 2015 our group first constructed “molecular volcano plots”<sup>1</sup> by examining a prototypical homogeneous catalysis reaction, Suzuki–Miyaura cross-coupling. This initial work opened a new research line aimed at, broadly speaking, identifying new and improved catalysts for relevant chemical problems by developing and expanding a computational framework based on creating and applying volcano plots to the study of homogeneous catalysis. This Account explores the key developments and chemical findings that constitute the emerging field of molecular volcano plots.

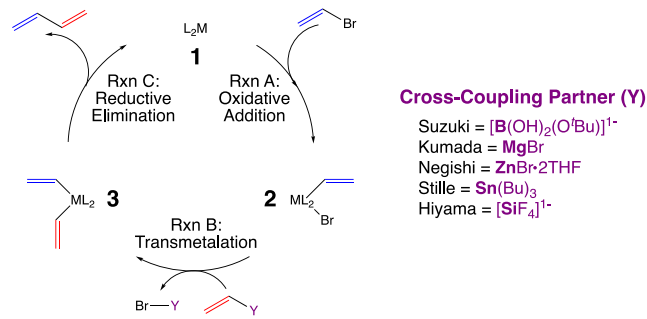
## THERMODYNAMIC VOLCANO PLOTS—PROOF OF CONCEPT

Our initial work<sup>1</sup> began by selecting a homogeneously catalyzed reaction with available experimental data that would serve as an important “check” on the validity of the results obtained from our yet-unproven molecular volcanoes. As a proof-of-principle example, we examined a Suzuki–Miyaura cross-coupling reaction of a vinyl bromide and a vinylboronic acid to form butadiene (eq 1). Invoking a typical heterogeneous/electrocatalysis protocol, we restricted our analysis only to thermodynamic aspects of the catalytic cycle (*i.e.*, intermediates only) for a



series of 36 catalysts comprising six metal centers (Ni, Pd, Pt, Cu, Ag, Au) appended with a set of six electronically diverse ligands. From this catalyst set, we identified robust LFESRs between the relative free energies of the different catalytic cycle intermediates, which were critical for constructing the corresponding molecular volcano. Ultimately, the relative energy of intermediate 2 with respect to the isolated catalyst and substrate (equivalent to oxidative addition; Scheme 1, Rxn 1)

**Scheme 1. Abbreviated Catalytic Cycle for C–C Cross-Coupling Reactions**



A) was found to be the best descriptor variable. Expressing each reaction energy in terms of the descriptor by postprocessing the LFESRs (see the Supporting Information of ref 1 for details) led to Figure 2a, where the descriptor variable is plotted along the  $x$

axis and the negative of the reaction free energy for the most difficult reaction step in the catalytic cycle (by convention termed the potential-determining step, pds) is given on the  $y$  axis. Adding the points for the 36 catalysts to the volcano showed that the results aligned well with experimental trends: palladium catalysts appear near the plateau while most other group 10 metal catalysts (nickel and platinum) are located along the volcano's strong-binding left slope (where the free energy of Rxn C is the costliest catalytic cycle step). On the other hand, all of the coinage-metal catalysts were found along the volcano's weak-binding right slope (where the free energy of Rxn A is the costliest catalytic cycle step), indicative of generally worse thermodynamic profiles than for the group 10 catalysts. Overall, the existence of unambiguous LFESRs, the reconstitution of a typical volcano shape, and the theoretical finding that experimentally verified catalysts lie atop the volcano validated that the volcano concept is applicable to homogeneous catalysis.

While our initial work established the viability of molecular volcano plots, a number of questions concerning their overall robustness and transferability persisted. In cross-coupling reactions, for instance, some catalysts (e.g., those with bulky ligands) likely transit the catalytic cycle in a monoligated state rather than a bisligated state (as examined in our original work). Moreover, it is also plausible that some catalysts exist in higher oxidation and/or alternative spin states, which would also influence their reactivity. This raises the following question: do these alterations lead to separate sets of LFESRs and unique volcano plots? To answer this question, we reexamined Suzuki–Miyaura cross-coupling, placing emphasis on how changes in the ligation, spin, or oxidation state influence both the accuracy of

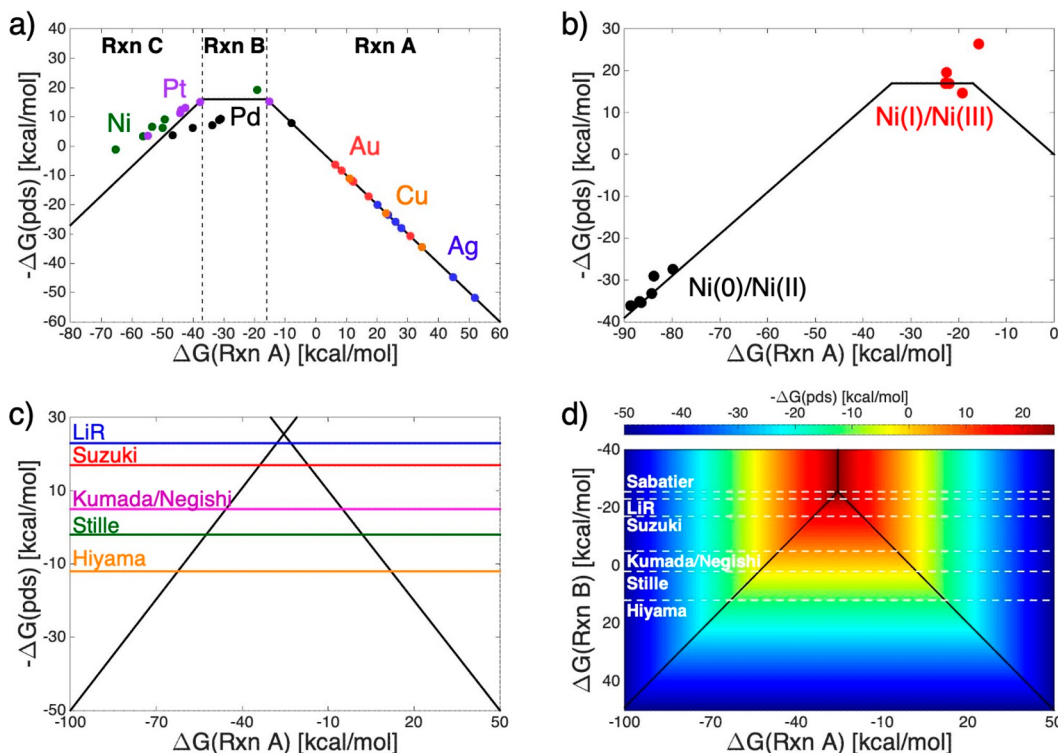
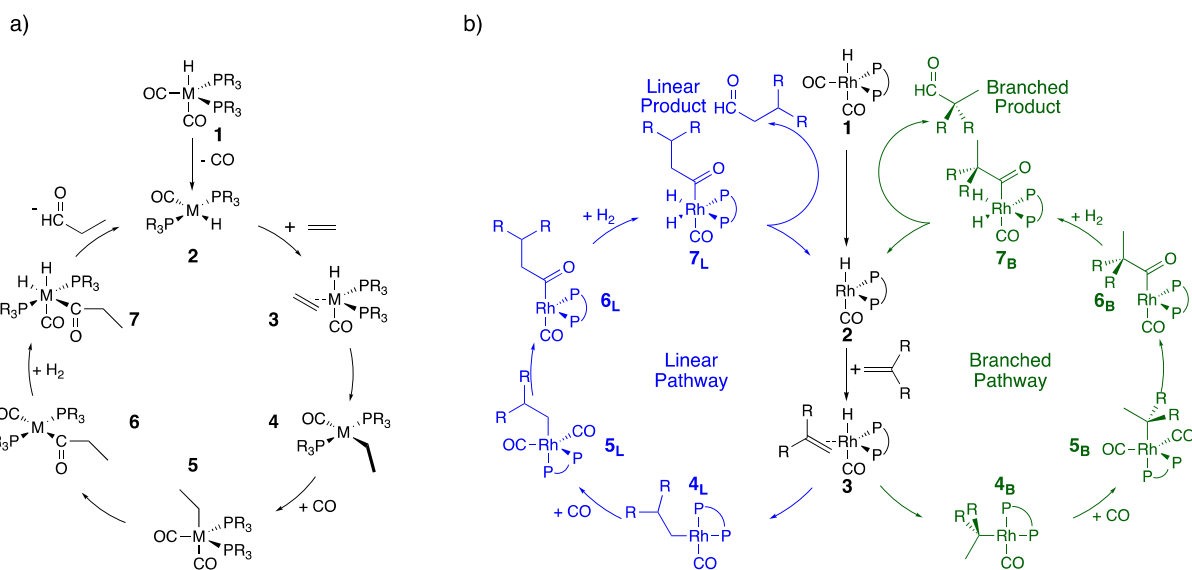


**Figure 2.** (a) Thermodynamic volcano plot for a Suzuki–Miyaura C–C cross-coupling reaction. (b) Volcano plot highlighting the thermodynamic influence induced by changes in oxidation state. It should be noted that the same linear free energy scaling relationships and volcano plot describe both sets of species. (c) Volcano plot depicting changes in the transmetalation energy from different named chemical reactions. (d) Three-dimensional volcano showing the energetic relationship of the different cross-coupling variants. Panel (a) is from ref 1. CC BY 3.0. Panel (b) is reproduced with permission from ref 29. Copyright 2018 Wiley-VCH. Panels (c) and (d) are from ref 30. Copyright 2017 American Chemical Society.

**Scheme 2. Proposed Catalytic Cycle for the Hydroformylation Reaction with (a) Ethylene, Leading to a Single Product,<sup>33</sup> and (b) a Substituted Substrate, Leading to Two Regiosomers<sup>34</sup>**



the LFESRs and the volcano shape.<sup>29</sup> We found that while the overall thermodynamic profiles of the catalysts change when the ligation, spin, or oxidation states are altered, the same sets of LFESRs remain. As a result, a single volcano describes catalysts with any (or all) of the aforementioned changes. This is nicely illustrated by the monoligated Ni catalysts shown in Figure 2b, which possess good thermodynamic profiles when traversing the catalytic cycle in the Ni(I)/Ni(III) oxidation states but are less active in their Ni(0)/Ni(II) states. Indeed, Figure 2b shows that moving from Ni(0)/Ni(II) to Ni(I)/Ni(III) weakens the interaction between the catalyst and the reaction intermediates, causing a rightward shift in the volcano plot that corresponds to improved thermodynamic profiles. However, it should be noted that the robustness of the LFESRs observed for C–C cross-coupling is not expected for all situations and reactions, particularly if the change of spin or oxidation state affects the performance of density functionals. For instance, for metal-oxo intermediates in the oxygen evolution reaction, we have shown that density functional approximations do not properly balance the effects brought on by static correlation and spurious electron delocalization.<sup>31</sup>

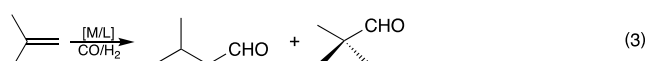
The previously described works applied molecular volcanoes to a Suzuki–Miyaura cross-coupling reaction. However, Suzuki–Miyaura coupling is only one of a number of “named” cross-coupling reactions (e.g., Kumada, Negishi, Stille, Hiyama) that differ only by the chemical agent employed during transmetalation (“Y” in Scheme 1, Rxn B). Indeed, the free energy associated with transmetalation is often the largest thermodynamic barrier encountered in the catalytic cycle for “good” catalysts (*i.e.*, this reaction defines the volcano plateau). Thus, altering the cross-coupling partner influences the energy of transmetalation that dictates the height of the volcano plateau (Figure 2c), where more reactive coupling partners (e.g., LiR) raise and less reactive partners (e.g., SiF<sub>4</sub><sup>-</sup>, Hiyama) lower the plateau height in the corresponding volcano plots.

Because a relationship exists between each of these individual cross-coupling volcanoes, we utilized a three-dimensional volcano plot (Figure 2d) to create a unified thermodynamic picture of cross-coupling reactions.<sup>30</sup> This three-dimensional volcano is most easily understood as a series of standard two-

dimensional volcanoes (e.g., Figure 2a) pasted together, where the descriptor variable is displayed on the *x* axis and  $-\Delta G(\text{pds})$  on the *z* axis. The three-dimensional volcano also uses the transmetalation energy as a second descriptor variable on the *y* axis. Knowing the value of the transmetalation step associated with a specific chemical reagent (e.g., SiF<sub>4</sub><sup>-</sup> for Hiyama coupling) reveals the location of the specific two-dimensional volcano “slice”. In this case, as the transmetalation step becomes easier (*i.e.*, moves toward more exergonic transmetalation energies), the value of the pds decreases (shifts from blue to green to red) (Figure 2d). This increase in the reaction’s thermodynamic drive is accompanied by a narrowing of the volcano plateau, meaning that fewer catalysts will have ideal thermodynamic profiles. Ultimately, the transmetalation becomes so energetically facile that the plateau disappears entirely (represented by the Sabatier line in Figure 2d), leaving only a peak where the energies of either reductive elimination (left slope) or oxidative addition (right slope) dictate the catalytic cycle thermodynamics. Overall, this generalized picture of C–C cross-coupling provides routes for improving the thermodynamics of any catalyst (*i.e.*, reducing the energy of the pds) by identifying the cross-coupling variant that leads to the most energetically balanced catalytic cycle. The three-dimensional volcano concept can also be used to examine other facets of homogeneous catalytic reactions, such as the energetic role played by the electrophilic coupling component in cross-coupling reactions.<sup>32</sup>

## ■ KINETIC VOLCANO PLOTS—PROOF OF CONCEPT

The molecular volcanoes described above considered only catalytic cycle thermodynamics. However, we knew that kinetics must also be considered to have a meaningful impact in homogeneous catalysis. With this in mind, we created “kinetic volcanoes”<sup>33</sup> by examining the industrially important hydroformylation reaction (eq 2 and Scheme 2a), which produces millions of tons of aldehyde annually, using a catalyst database created by combining eight metal centers from groups 8–10 with four monodentate phosphine ligands having different steric parameters (PPh<sub>3</sub>, PMe<sub>3</sub>, PPh<sub>3</sub>, and PCy<sub>3</sub>). This work showed that transition state barriers could be predicted with acceptable



accuracy directly from the descriptor variable and reproduced experimental trends with Rh catalysts found near the volcano peak (Figure 3a). A closer examination of the LFESRs revealed that differences in ligand bulk led to slightly different sets of scaling relationships. By constructing separate volcanoes for each ligand, we demonstrated that increasing steric bulk reduces the key transition state barrier (*i.e.*, the largest energy difference between a connected intermediate and transition state found in the catalytic cycle, termed the kinetic-determining step, kds) and leads to more active catalysts (Figure 3b). Furthermore, establishing relationships between the peaks of the different volcanoes and a measure of steric bulk led to simple structure–activity relationships that estimated the height of the volcano peak (corresponding to anticipated catalytic activity) for any phosphine ligand from the Tolman cone angle.

Eager to expand the utility of kinetic volcanoes, we revisited the hydroformylation reaction by probing the ability of volcanoes to predict product regioselectivity, an aspect of clear interest to experimentalists.<sup>34</sup> Our initial application used ethylene as the substrate, which leads to a single product (eq 2). To introduce regioselectivity, 2-methylpropene was used as the substrate (eq 3), which yields branched (2,2-dimethylpropanal) and linear (3-methylbutanal) regioisomers (Scheme 2b). In addition to identifying active catalysts (*i.e.*, those with low transition state barriers) directly from a descriptor variable, we also wanted to accurately predict the reaction's regioisomeric excess (*re*). This represents a challenging task given the sensitivity of the *re* to small changes in the free energy differences between product-distinguishing transition states. Since identifying highly accurate LFESRs was key, we restricted our analysis to rhodium catalysts bearing bidentate phosphine ligands. Ultimately, two volcano plots were constructed [one for the linear product (blue) and one for the branched (green) product; Figure 4a] that estimated both catalytic activity and selectivity through the use of two descriptor variables. Remarkably, of 10 catalysts predicted to be highly selective (*i.e.*, *re* > 95), nine had similar *re* values when the free energy differences of the transition states that dictate regioselectivity were directly computed. After construction, the volcano plots

were used to screen a database of 68 additional ligands to search for active species that selectively form the more elusive branched regioisomer, which ultimately identified several promising ligands (Figure 4b).

Despite the utility of the kinetic volcanoes, we remained interested in creating stronger links with experiment, where theoretical estimations of catalytic activity could be directly compared to experimental observables. An ideal quantity to accomplish this feat is the turnover frequency (TOF), as defined in eq 4:

$$\text{TOF} = \frac{N}{[C]t} \approx \frac{k_B T}{h} e^{-\delta E/RT} \quad (4)$$

One way to achieve this is to use the energy span model of Kozuch and Shaik<sup>35–37</sup> to convert a computed catalytic cycle free energy profile into a theoretical TOF (eq 4) by measuring its “energy span”  $\delta E$  (eq 5):

$$\delta E = \max_{i,j}(T_i - I_j + \delta G_{ij}) \quad (5)$$

where  $T_i$  is the energy of the turnover-determining transition state (TDTS) (*i.e.*, the rate-limiting TS),  $I_j$  is the turnover-determining intermediate (TDI) (*i.e.*, the most populated intermediate), and  $\delta G_{ij}$  is a correction for the cyclic nature of the catalytic cycle.<sup>38</sup> In contrast to earlier volcanoes, where only the free energy differences between intermediates and transition states (or intermediates and other intermediates for thermodynamic volcanoes) directly linked in the catalytic cycle were measured, the energy span model assesses the TDI and TDTS of the entire catalytic cycle. Thus, all intermediate/transition state combinations are checked to identify the largest energy span. Since we already established that a descriptor variable can predict the relative energies of all intermediates and transition states through LFESRs, we can estimate the energy span for any prospective catalyst and plot the theoretical TOF (*i.e.*, number of catalytic cycles completed per second) as a function of the descriptor variable, resulting in a TOF volcano.<sup>3</sup> Figure 5 compares a traditional energy-based volcano (Figure 5a) to the corresponding TOF volcano (Figure 5b) for the conversion of  $\text{CO}_2$  and  $\text{H}_2$  to formate using transition metal pincer complexes (eq 6). In addition to directly relating to experimental

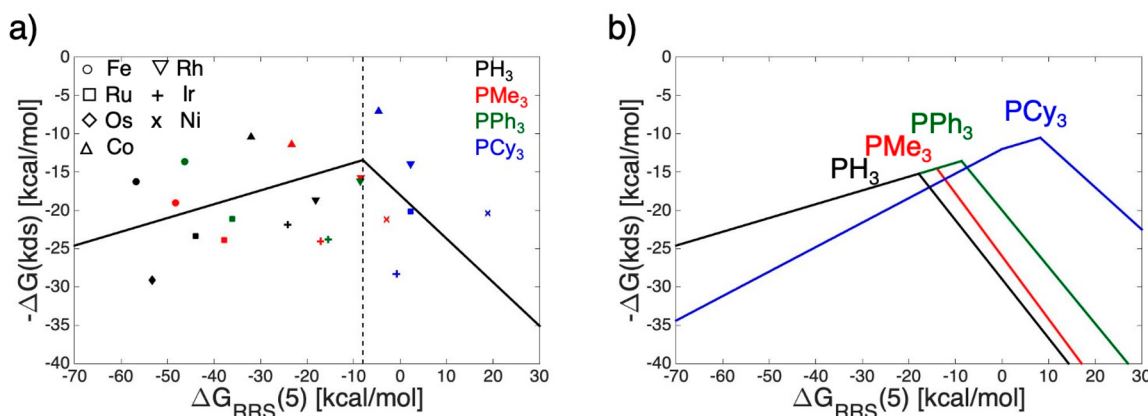


**Figure 3.** (a) Kinetic volcano plot for the hydroformylation reaction using ethylene as a substrate. (b) Ligands separated by sterics reveal increasing bulk yields a higher volcano that corresponds to a catalytic cycle with lower free energy barriers. From ref 33. CC BY-NC 3.0.

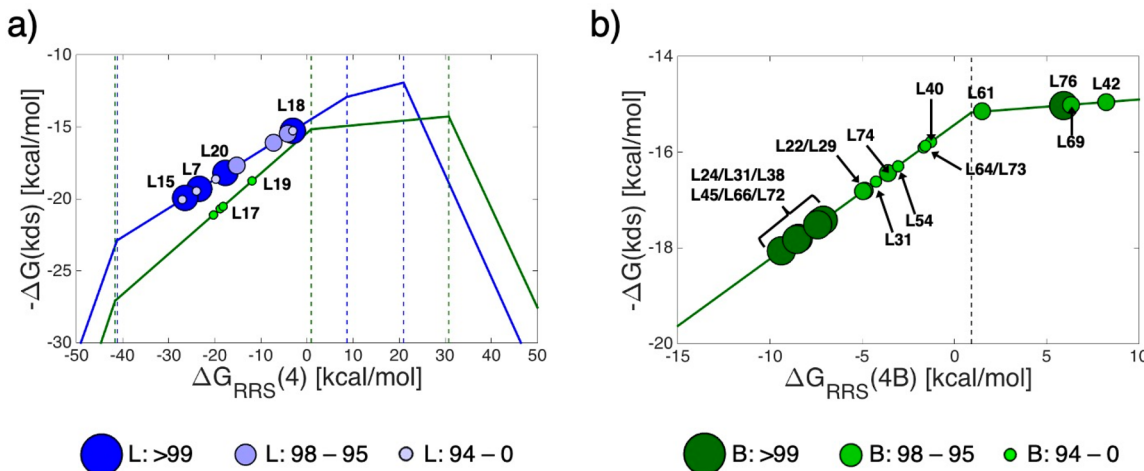


**Figure 4.** (a) Regioselective molecular volcano plots [linear product (blue), branched product (green)] for the hydroformylation reaction. Circle size indicates the range of *re* values for each catalyst according to the provided color codes. (b) Screening for catalysts that selectively form the branched product revealed several ligands with predicted *re* values greater than 90. The “L” values correspond to ligands in the original work. Reproduced with permission from ref 34. Copyright 2018 Wiley-VHCA.

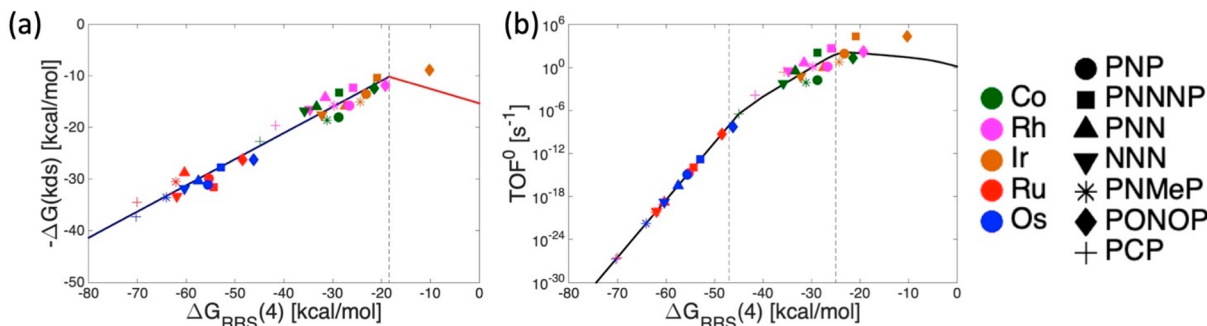


**Figure 5.** (a) Energy-based volcano plot and (b) TOF volcano plot for the catalytic formation of formate from  $\text{CO}_2$  and  $\text{H}_2$ . Reproduced from ref 3. Copyright 2019 American Chemical Society.

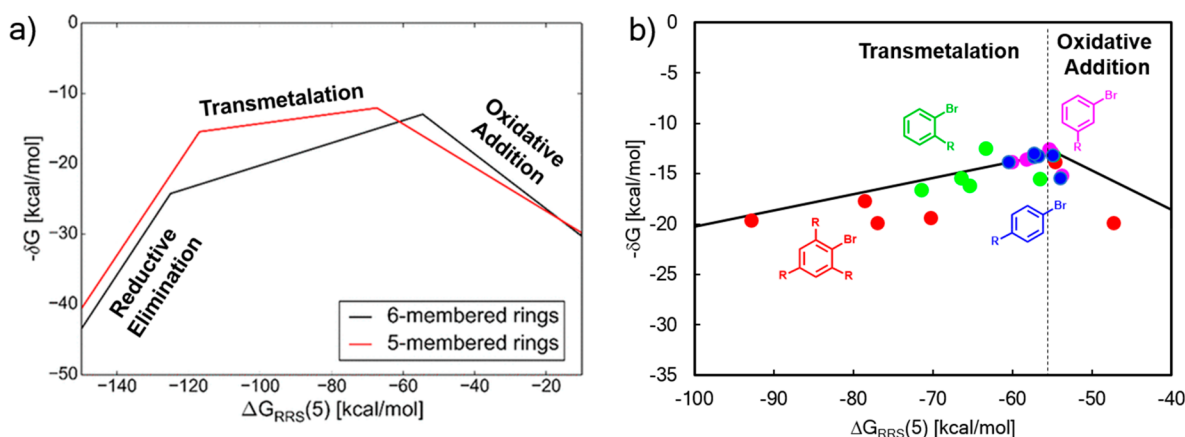


**Figure 6.** (a) Substrate volcano plots made from six-membered-ring (black) and five-membered-ring (red) substrates for a Suzuki–Miyaura cross-coupling reaction and (b) detailed plot showing how electronic and steric elements influence the energy of the catalytic cycle. Reproduced from ref 39. Copyright 2020 American Chemical Society.

measurements, the TOF volcano also reveals additional features that are more ambiguous in energy-based volcanoes. For instance, Figure 5b shows a rapid decline in catalytic activity when moving from the volcano top to more negative descriptor values (*i.e.*, moving leftward), while catalysts having descriptor values located to the right of the volcano top retain greater catalytic activity. Overall, TOF volcanoes represent a computa-

tional tool that is useful to experimentalists because it provides a quickly determined estimation of the TOF for any catalyst prior to synthesis.

All of the previously discussed works used molecular volcanoes to estimate catalytic performance. Recently, we moved beyond catalyst screening and highlighted how volcanoes can be used to analyze a reaction’s substrate scope.<sup>39</sup>

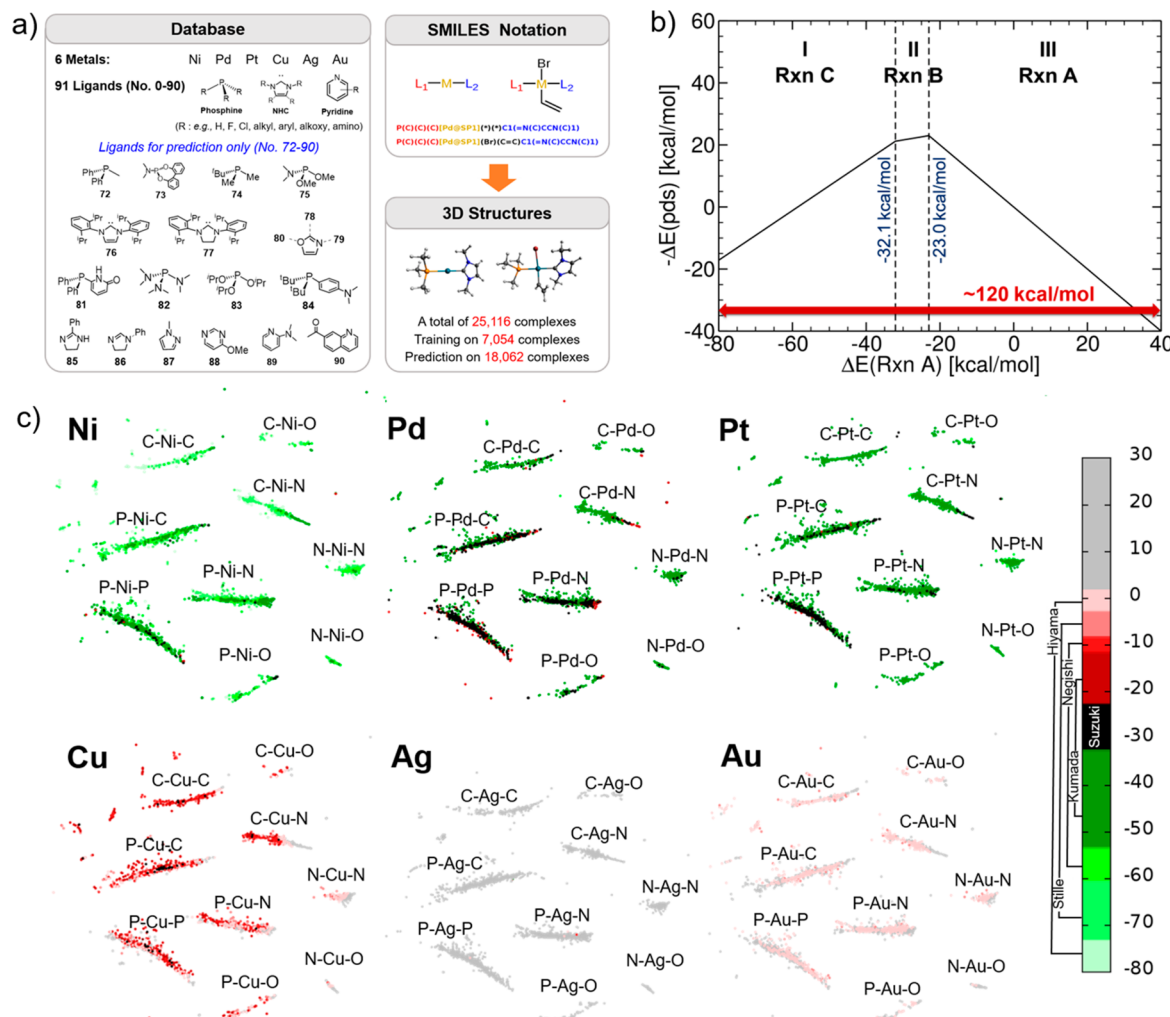


**Figure 7.** (a) Schematic of database construction for ML. (b) Volcano plot for Suzuki–Miyaura cross-coupling used to define the plateau range representing ideal catalysts. (c) Sketch maps of each metal colored by the value of the energy descriptor variable [ $\Delta E(\text{Rxn A})$ , in kcal/mol]. Each group corresponds to different metal–ligand combination (P = phosphine, C = carbene, N = pyridine, O = oxazole). Panels (a) and (b) are from ref 2. CC BY-NC 3.0. Panel (c) is reproduced with permission from ref 40. Copyright 2019 Wiley-VCH.

Understanding the breadth of substrate reactivity is a crucial component of experimental research, and thus, computational tools aimed at probing this often-overlooked aspect of chemistry are welcome. To accomplish this, we assessed how changing the substrate varied the catalytic cycle energetics by examining a series of electrophile reactants (aryl bromides) possessing differing skeletal, electronic, and steric components for Suzuki–Miyaura cross-coupling with a single catalyst,  $\text{Pd}(\text{PPh}_3)_4$ . These “substrate volcanoes” uncovered a detailed picture of the energetic interplay between steric and electronic properties. Specifically, different core structures lead to unique volcano plots (Figure 6a), mainly based on modulation of the electronic properties. Further, we saw that steric influences played a major role in dictating the energetics of transmetalation (Figure 6b), while oxidative addition was more heavily influenced by electronic factors. With the better understanding of how substrates and catalysts interact with one another provided by tools of this type, the catalytic cycle energetics can be tuned for any substrate by selecting an appropriate catalyst, which represents an additional aspect of volcano plots that should lead to more targeted experimental studies. In the future, we envision placing greater emphasis on these substrate volcanoes.

## TOWARD BIGGER DATA/MACHINE LEARNING

Over the past several years, “big data”-oriented chemical studies have begun to appear with greater frequency, an aspect that has coincided with the increasing use of machine learning (ML) applications. An underlying idea of volcano plots is that after the volcano plot is constructed, the performance of any prospective catalyst can be quickly established by determining the value of the descriptor variable. In this sense, volcano plots already represent a route toward big(ger) data analytics, where hundreds of species can be analyzed through a handful of DFT computations. Nonetheless, further upscaling (to reach 10000+ catalysts) still requires bypassing the computational bottleneck associated with determining the descriptor variable. To overcome this, in collaboration with the von Lilienfeld group, we employed ML models to directly predict values of the catalyst descriptor variable for a Suzuki cross-coupling reaction (eq 1).<sup>2</sup> To accomplish this, a kernel ridge regression-based ML model was trained on 7054 catalysts derived from the database shown in Figure 7a and yielded predictions of the descriptor variable with a mean absolute error (MAE) of only 2.73 kcal/mol. Using these ML-determined descriptor variables together with a preconstructed volcano plot (Figure 7b), we estimated the

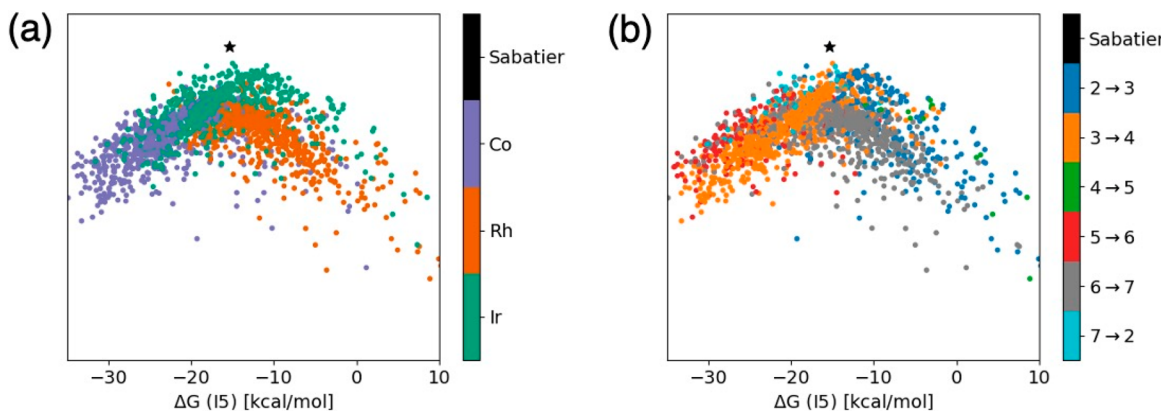


**Figure 8.** Augmented volcano plots for the thermodynamics of the hydroformylation reaction (eq 2) colored by (a) the metal center of the catalyst and (b) the most thermodynamically difficult reaction step. The  $y$  value for each catalyst is a measurement of similarity to the ideal reference catalyst (depicted as a black star). From ref 4. CC BY-NC 3.0.

catalytic cycle thermodynamics of over 18 000 out-of-sample catalysts and ultimately identified 557 possessing optimal thermodynamics (*i.e.*, lying on the volcano plateau).

After demonstrating the successful coupling of volcano plots and ML for the Suzuki cross-coupling reaction<sup>2</sup> and having previously demonstrated the thermodynamic link between Suzuki and other types of cross-coupling reactions,<sup>30</sup> we undertook a data-mining study using 25 116 catalysts in our cross-coupling database (constituting the training and test sets discussed above) with the objective of better understanding the underlying chemistry. To accomplish this, a dimensionality reduction algorithm (sketch map)<sup>41,42</sup> was employed to unravel the effects of both the metal and the ligand. On the basis of the chemical and structural details of each complex, individual sketch maps were created for catalysts bearing the same metal. These sketch maps then subdivided the set of metal complexes into groups based on the metal–ligand connectivity (Figure 7c).<sup>40</sup> Because the thermodynamics of the various cross-coupling reactions are interrelated by a 3D volcano (Figure 2d), the point representing each catalyst was colored according to the cross-coupling reaction for which it had ideal thermodynamics (*i.e.*, black for Suzuki, darker to lighter green/red shades for Kumada, Negishi, Stille, Hiyama, respectively). The colors in Figure 7c illustrate the behavior induced by each metal, showing that group 10 species (Ni, Pd, Pt) often make better catalysts than group 11 metals (Cu, Ag, Au). Diving deeper into the data reveals how the ligand type affects the value of the descriptor variable. For instance, phosphines polarize the metal complexes, causing group 10 and 11 metals to have similar energetic patterns, while pyridine ligands induce an opposing effect, causing group 10 and 11 catalysts to have distinctly different energy profiles. Overall, big-data-type analyses uncover broad trends regarding catalyst behavior that would likely remain hidden in analyses of only a small amount of data. In turn, this not only provides specific examples of catalysts possessing desirable properties but also reveals those features likely to be important when choosing a family of catalysts to examine for a specific reaction. We believe that the volcano plot/ML tandem represents an important milestone in the ability to quickly generate large quantities of data that can subsequently be mined using tools such as dimensionality reduction algorithms. Together, these tools represent a unique route to apply data science approaches to

study homogeneous catalysis, which should propel new explorations of catalysis space.

Big-data approaches not only accelerate the screening process but also can be used to create new types of molecular volcanoes. Very recently, we introduced “augmented volcano plots”<sup>4</sup> that differ conceptually from typical molecular volcanoes in both their construction and how the catalytic activity is measured. Rather than relying on LFESRs to construct the volcano shape by plotting a single reaction energy as a function of the descriptor variable to represent the catalytic cycle thermodynamics, in augmented volcanoes the energy of the entire catalytic cycle of each species is compared to an ideal reference species (such as the Sabatier ideal profile) using a dimensionality reduction algorithm. The resulting global “similarity measure” can then be plotted as a function of the descriptor variable, which results in an augmented volcano [shown here for the thermodynamics of the hydroformylation reaction (eq 2)]. This unique volcano type identifies catalysts with the best energy profiles [which appear near the ideal, Sabatier, reference point (Figure 8a)] and reveals the multiple sets of scaling relationships that control the catalytic process (Figure 8b). Overall, augmented volcanoes represent another tool that allows trends that may be obscured in traditional molecular volcanoes (*e.g.*, the ameliorated thermodynamics of iridium shown in Figure 8a) and the importance of multiple reaction steps in establishing overall catalyst quality (as shown by the presence of orange, red, and light-blue points on the left side of Figure 8b) to be identified.

## ■ APPLICATIONS TO SPECIFIC CHEMICAL PROBLEMS

The preceding sections highlighted the various molecular volcano plot flavors, yet the application of these tools to unravel the interesting chemistry catalyzed by homogeneous species is also important. Below we feature three selected applications: the hydrogenation of CO<sub>2</sub> to formate using transition metal pincer catalysts,<sup>43</sup> aryl ether cleavage using nickel catalysts,<sup>44</sup> and molecular water oxidation catalysts.<sup>31</sup> Aside from these selected works, other groups have also used linear scaling relationships and volcano plots in homogeneous settings. This includes examining reactions such as water oxidation,<sup>45,46</sup> N<sub>2</sub> reduction,<sup>47</sup> C–N coupling,<sup>48</sup> asymmetric hydrogenation of ketones,<sup>49</sup> oxygen reduction,<sup>50</sup> and others.<sup>51–54</sup> Notably, three

perspective articles<sup>55–57</sup> have recently appeared in the literature that partially touch on aspects of the above work.

The hydrogenation of carbon dioxide to C<sub>1</sub> compounds is an intriguing route for the production of chemical feedstocks. Toward this end, we used molecular volcano plots to examine the catalytic hydrogenation of CO<sub>2</sub> to formate (eq 6). The volcanoes revealed the influence of each catalyst component and suggested a straightforward route to enhance the activity by coupling group 9 transition metals (Ir, Rh, Co) with  $\pi$ -acidic pincer ligands.<sup>43</sup> The strong  $\pi$ -acceptor ligand facilitates more facile heterolytic cleavage of H<sub>2</sub>, which is the rate-determining step in the catalytic cycle.

Reductive cleavage of the C–O bond in aryl ether complexes can be used to create chemical feedstocks from renewable resources.<sup>44</sup> In this work, a volcano plot/ML tandem approach (similar to Figure 7a) was used to predict the activity of 143 000 nickel catalysts bearing phosphine and carbene ligands for the reaction shown in eq 7. The distribution of descriptor values

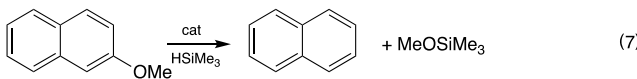


(Figure 9a) revealed that neither phosphine nor carbene ligands are ideally suited to catalyze this reaction. However, several phosphine species lying in the leftmost tail of the blue distribution were identified as promising candidates. Analysis of the geometries of key catalytic cycle intermediates revealed assorted non-covalent interactions that modulate the binding of the substrate/product with the catalyst, which leads to a more energetically facile catalytic process.

Solid-state and molecular water oxidation catalysts have been well-studied individually by computation, yet a unified energetic picture is lacking. To better comprehend the similarities and differences between these two types of catalysts, we created volcano plots that revealed a dissimilarity in the LFESRs of \*–OH and \*=O species and corresponding unique shapes for the solid-state and molecular volcano curves.<sup>31</sup> While the solid-state volcano (orange dashed line in Figure 9b) has a sharp peak, the molecular variant (black solid line in Figure 9b) has a broad plateau, indicating that a large number of molecular catalysts should have ideal reaction thermodynamics.

## CONCLUSION

This Account has provided an overview of the unique types of molecular volcano plots ranging from proof-of-concept origins to the latest variants incorporating aspects of big data and machine learning. Since 2015, we have steadily introduced new theoretical refinements aimed at crafting a set of comprehensive tools tailored to address key aspects of homogeneous catalysis such as predicting the kinetic profiles of species, creating unified pictures of reaction classes, addressing issues of product selectivity, and integrating aspects of machine learning and big-data analysis. Although much of the work has focused on deriving the theoretical framework of molecular volcanoes, we hope that this Account serves as an inspiration to other researchers to apply these tools to their own interesting catalytic reactions, particularly in situations where theoretical predictions can lead to experimental testing and verification. While the computational toolbox we have built already addresses many aspects of the behavior of homogeneous catalysts,<sup>58</sup> it will be particularly interesting to see how the latest emerging methods from big data and machine learning can be incorporated into future volcanoes to both improve their predictive ability and enhance their utility in data mining to achieve greater chemical understanding.

## AUTHOR INFORMATION

### Corresponding Author

Clemence Corminboeuf – *Laboratory for Computational Molecular Design, Institute of Chemical Sciences and Engineering and National Centre for Computational Design and Discovery of Novel Materials (MARVEL), Ecole Polytechnique Fédérale de Lausanne (EPFL), 1015 Lausanne, Switzerland;* [orcid.org/0000-0001-7993-2879](https://orcid.org/0000-0001-7993-2879); Email: [clemence.corminboeuf@epfl.ch](mailto:clemence.corminboeuf@epfl.ch)

### Authors

Matthew D. Wodrich – *Laboratory for Computational Molecular Design, Institute of Chemical Sciences and Engineering, Ecole Polytechnique Fédérale de Lausanne (EPFL), 1015 Lausanne, Switzerland;* [orcid.org/0000-0002-6006-671X](https://orcid.org/0000-0002-6006-671X)

Boosarun Sawatlon – *Laboratory for Computational Molecular Design, Institute of Chemical Sciences and Engineering, Ecole Polytechnique Fédérale de Lausanne*

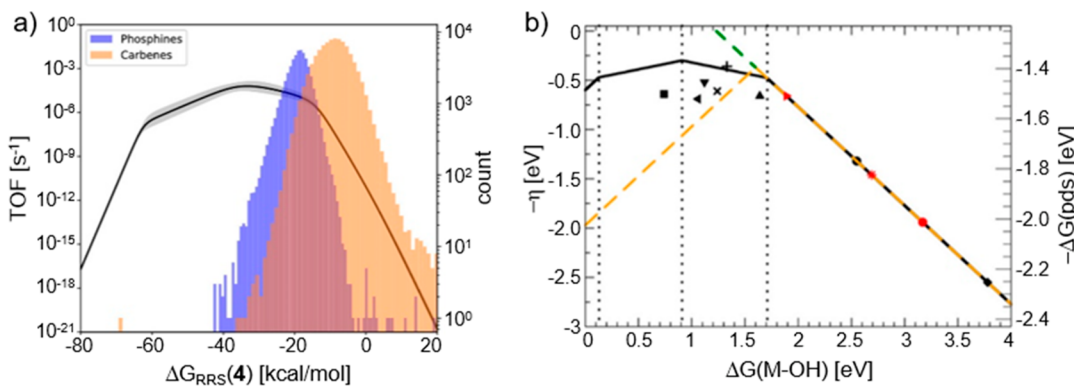


**Figure 9.** (a) Distribution of descriptor values and their location on the TOF volcano plot of reductive C–O cleavage of an aryl ether. (b) Comparison of the molecular volcano plot (black line) and solid-state volcano plot (orange dashed line) for the oxygen evolution reaction (OER).  $\eta$  is the overpotential, and  $\Delta G(pds)$  is the redox potential of the potential-determining step [ $\eta = \Delta G(pds) - 1.23$  eV]. Reproduced from (a) ref 44 and (b) ref 31. Copyright 2020 and 2018, respectively, American Chemical Society.

(EPFL), 1015 Lausanne, Switzerland; [orcid.org/0000-0002-1600-022X](https://orcid.org/0000-0002-1600-022X)

**Michael Busch** — *Laboratory for Computational Molecular Design, Institute of Chemical Sciences and Engineering and National Centre for Computational Design and Discovery of Novel Materials (MARVEL), Ecole Polytechnique Fédérale de Lausanne (EPFL), 1015 Lausanne, Switzerland; Department of Chemistry and Materials Science, School of Chemical Engineering, Aalto University, 02150 Espoo, Finland*

Complete contact information is available at:  
<https://pubs.acs.org/10.1021/acs.accounts.0c00857>

## Notes

The authors declare no competing financial interest.

## Biographies

**Matthew D. Wodrich** was born in Mesa, Arizona, USA, and earned B.S. and Ph.D. degrees from the University of Arizona in 2002 and the University of Georgia in 2006, respectively. After several postdoctoral positions in Switzerland, in 2015 he obtained a research scientist position at École Polytechnique Fédérale de Lausanne (EPFL). His current research interests lie in developing and applying computational tools to better understand and identify new homogeneous catalysts.

**Boodsarin Sawatlon** was born in Rayong, Thailand, and received her B.S. and M.Sc. degrees in chemistry from Mahidol University in Thailand. In 2017 she moved to Lausanne, Switzerland, to join the group of Clémence Corminboeuf at EPFL as a Ph.D. student. Her research involves developing and applying molecular volcano plots to homogeneous catalysis with the aim of uncovering general chemical trends and proposing new catalytic species.

**Michael Busch** was born in Kaufbeuren, Germany. He received his diploma in chemistry from Ulm University in 2008 and his Ph.D. from the University of Gothenburg in 2012. In the following years he was a postdoctoral researcher at the Technical University of Denmark (DTU), EPFL, and Chalmers University of Technology. In 2018 he joined Nouryon as a project scientist to study fundamental aspects of the industrial electrosynthesis of chlorate. Currently he is a postdoctoral researcher at Aalto University. His research interests include fundamental and applied computational electrochemistry, photoelectrochemistry, homogeneous catalysis, and surface science.

**Clemence Corminboeuf** was born in Geneva, Switzerland, and earned her B.S., M.S., and Ph.D. degrees from the University of Geneva, followed by postdoctoral positions at New York University and the University of Georgia. In 2007 she began her independent career at EPFL as an assistant professor and was subsequently promoted to associate professor in 2014 and full professor in 2019. Her research focuses on developing electronic structure methods and creating conceptual tools targeted at organic electronics and homogeneous catalysis.

## ACKNOWLEDGMENTS

The authors thank Dr. Benjamin Meyer and Dr. Alberto Fabrizio, whose work on molecular volcanoes is included in this Account. We also thank our external collaborators, Mr. Stefan Heinen and Prof. O. Anatole von Lilienfeld (University of Basel) as well as Dr. Ephrat Solel and Prof. Sebastian Kozuch (Ben-Gurion University of the Negev) for their contributions. Mr. Raimon Fabregat is acknowledged for assistance with the conspectus graphic. Funding was provided by the National Centre for Competence in Research (NCCR) Materials Revolution: Computational Design and Discovery of Novel

Materials (MARVEL) of the Swiss National Science Foundation (SNSF Grant 200020\_175496) and the EPFL, who are acknowledged.

## REFERENCES

- 1) Busch, M.; Wodrich, M. D.; Corminboeuf, C. Linear Scaling Relationships and Volcano Plots in Homogeneous Catalysis – Revisiting the Suzuki Reaction. *Chem. Sci.* **2015**, *6*, 6754–6761.
- 2) Meyer, B.; Sawatlon, B.; Heinen, S.; von Lilienfeld, O. A.; Corminboeuf, C. Machine Learning Meets Volcano Plots: Computational Discovery of Cross-Coupling Catalysts. *Chem. Sci.* **2018**, *9*, 7069–7077.
- 3) Wodrich, M. D.; Sawatlon, B.; Solel, E.; Kozuch, S.; Corminboeuf, C. Activity-Based Screening of Homogeneous Catalysts through the Rapid Assessment of Theoretically Derived Turnover Frequencies. *ACS Catal.* **2019**, *9*, 5716–5725.
- 4) Wodrich, M. D.; Fabrizio, A.; Meyer, B.; Corminboeuf, C. Data-Powered Augmented Volcano Plots for Homogeneous Catalysis. *Chem. Sci.* **2020**, *11*, 12070–12080.
- 5) Sabatier, P. Hydrogénations et Déhydrogénations Par Catalyse. *Ber. Dtsch. Chem. Ges.* **1911**, *44*, 1984–2001.
- 6) Sabatier, P. *La Catalyse en Chimie Organique*; Librairie Polytechnique: Paris, 1913.
- 7) Gerischer, H. Mechanismus Der Elektrolytischen Wasserstoffabscheidung Und Adsorptionsenergie von Atomarem Wasserstoff. *Bull. Soc. Chim. Belg.* **1958**, *67*, 506–527.
- 8) Parsons, R. The Rate of Electrolytic Hydrogen Evolution and the Heat of Adsorption of Hydrogen. *Trans. Faraday Soc.* **1958**, *54*, 1053–1063.
- 9) Trasatti, S. Work Function, Electronegativity, and Electrochemical Behaviour of Metals: III. Electrolytic Hydrogen Evolution in Acid Solutions. *J. Electroanal. Chem. Interfacial Electrochem.* **1972**, *39*, 163–184.
- 10) Trasatti, S. Electrocatalysis in the Anodic Evolution of Oxygen and Chlorine. *Electrochim. Acta* **1984**, *29*, 1503–1512.
- 11) Balandin, A. A. The Nature of Active Centers and the Kinetics of Catalytic Dehydrogenation. *Adv. Catal.* **1958**, *10*, 96–129.
- 12) Vijh, A. K. Sabatier-Balandin Interpretation of the Catalytic Decomposition of Nitrous Oxide on Metal-Oxide Semiconductors. *J. Catal.* **1973**, *31*, 51–54.
- 13) Vannice, M. A. The Catalytic Synthesis of Hydrocarbons from Mixtures over the Group VIII Metals: V. The Catalytic Behavior of Silica-Supported Metals. *J. Catal.* **1977**, *50*, 228–236.
- 14) Somorjai, G. A. Modern Concepts in Surface Science and Heterogeneous Catalysis. *J. Phys. Chem.* **1990**, *94*, 1013–1023 and references cited therein.
- 15) Ichikawa, S. Volcano-Shaped Curves in Heterogeneous Catalysis. *Chem. Eng. Sci.* **1990**, *45*, 529–535 and references cited therein.
- 16) Dumesic, J. A.; Huber, G. W.; Boudart, M. Principles of Heterogeneous Catalysis. In *Handbook of Heterogeneous Catalysis*; Wiley-VCH: Weinheim, Germany, 2008 and references cited therein.
- 17) Nørskov, J. K.; Rossmeisl, J.; Logadottir, A.; Lindqvist, L.; Kitchin, J. R.; Bligaard, T.; Jónsson, H. Origin of the Overpotential for Oxygen Reduction at a Fuel-Cell Cathode. *J. Phys. Chem. B* **2004**, *108*, 17886–17892.
- 18) Bligaard, T.; Nørskov, J. K.; Dahl, S.; Matthiesen, J.; Christensen, C. H.; Sehested, J. The Brønsted–Evans–Polanyi Relation and the Volcano Curve in Heterogeneous Catalysis. *J. Catal.* **2004**, *224*, 206–217.
- 19) Nørskov, J. K.; Bligaard, T.; Logadottir, A.; Kitchin, J. R.; Chen, J. G.; Pandelov, S.; Stimming, U. Trends in the Exchange Current for Hydrogen Evolution. *J. Electrochem. Soc.* **2005**, *152*, J23–J26.
- 20) Ferrin, P.; Simonetti, D.; Kandoi, S.; Kunke, E.; Dumesic, J. A.; Nørskov, J. K.; Mavrikakis, M. Modeling Ethanol Decomposition on Transition Metals: A Combined Application of Scaling and Brønsted–Evans–Polanyi Relations. *J. Am. Chem. Soc.* **2009**, *131*, 5809–5815.
- 21) Calle-Vallejo, F.; Martínez, J. I.; García-Lastra, J. M.; Rossmeisl, J.; Koper, M. T. M. Physical and Chemical Nature of the Scaling

- Relations between Adsorption Energies of Atoms on Metal Surfaces. *Phys. Rev. Lett.* **2012**, *108*, 116103.
- (22) Nørskov, J. K.; Bligaard, T.; Logadottir, A.; Bahn, S.; Hansen, L. B.; Bollinger, M.; Bengaard, H.; Hammer, B.; Sljivancanin, Z.; Mavrikakis, M.; Xu, Y.; Dahl, S.; Jacobsen, C. J. H. Universality in Heterogeneous Catalysis. *J. Catal.* **2002**, *209*, 275–278.
- (23) Rossmeisl, J.; Qu, Z.-W.; Zhu, H.; Kroes, G.-J.; Nørskov, J. K. Electrolysis of Water on Oxide Surfaces. *J. Electroanal. Chem.* **2007**, *607*, 83–89.
- (24) Man, I. C.; Su, H.-Y.; Calle-Vallejo, F.; Hansen, H. A.; Martínez, J. I.; Inoglu, N. G.; Kitchin, J.; Jaramillo, T. F.; Nørskov, J. K.; Rossmeisl, J. Universality in Oxygen Evolution Electrocatalysis on Oxide Surfaces. *ChemCatChem* **2011**, *3*, 1159–1165.
- (25) Exner, K. S. Recent Advancements Towards Closing the Gap between Electrocatalysis and Battery Science Communities: The Computational Lithium Electrode and Activity–Stability Volcano Plots. *ChemSusChem* **2019**, *12*, 2330–2344.
- (26) Busch, M.; Halck, N. B.; Kramm, U. I.; Siahrostami, S.; Krtík, P.; Rossmeisl, J. Beyond the Top of the Volcano? – A Unified Approach to Electrocatalytic Oxygen Reduction and Oxygen Evolution. *Nano Energy* **2016**, *29*, 126–135.
- (27) Busch, M. Water Oxidation: From Mechanisms to Limitations. *Curr. Opin. Electrochem.* **2018**, *9*, 278–284.
- (28) Swiegers, G. *Mechanical Catalysis: Methods of Enzymatic, Homogeneous, and Heterogeneous Catalysis*; John Wiley & Sons: Hoboken, NJ, 2008.
- (29) Wodrich, M. D.; Sawatlon, B.; Busch, M.; Corminboeuf, C. On the Generality of Molecular Volcano Plots. *ChemCatChem* **2018**, *10*, 1586–1591.
- (30) Busch, M.; Wodrich, M. D.; Corminboeuf, C. A Generalized Picture of C–C Cross-Coupling. *ACS Catal.* **2017**, *7*, 5643–5653.
- (31) Busch, M.; Fabrizio, A.; Luber, S.; Hutter, J.; Corminboeuf, C. Exploring the Limitation of Molecular Water Oxidation Catalysts. *J. Phys. Chem. C* **2018**, *122*, 12404–12412.
- (32) Busch, M.; Wodrich, M. D.; Corminboeuf, C. Improving the Thermodynamic Profiles of Prospective Suzuki–Miyaura Cross-Coupling Catalysts by Altering the Electrophilic Coupling Component. *ChemCatChem* **2018**, *10*, 1592–1597.
- (33) Wodrich, M. D.; Busch, M.; Corminboeuf, C. Accessing and Predicting the Kinetic Profiles of Homogeneous Catalysts from Volcano Plots. *Chem. Sci.* **2016**, *7*, 5723–5735.
- (34) Wodrich, M. D.; Busch, M.; Corminboeuf, C. Expedited Screening of Active and Regioselective Catalysts for the Hydroformylation Reaction. *Helv. Chim. Acta* **2018**, *101*, e1800107.
- (35) Kozuch, S.; Shaik, S. How to Conceptualize Catalytic Cycles? The Energetic Span Model. *Acc. Chem. Res.* **2011**, *44*, 101–110.
- (36) Kozuch, S. A Refinement of Everyday Thinking: The Energetic Span Model for Kinetic Assessment of Catalytic Cycles. *WIREs Comput. Mol. Sci.* **2012**, *2*, 795–815.
- (37) Solel, E.; Tarannam, N.; Kozuch, S. Catalysis: Energy Is the Measure of All Things. *Chem. Commun.* **2019**, *55*, 5306–5322.
- (38) A more comprehensive description of nomenclature and further discussion on determining theoretical TOFs are provided in ref 35.
- (39) Sawatlon, B.; Wodrich, M. D.; Corminboeuf, C. Probing Substrate Scope with Molecular Volcanoes. *Org. Lett.* **2020**, *22*, 7936–7941.
- (40) Sawatlon, B.; Wodrich, M. D.; Meyer, B.; Fabrizio, A.; Corminboeuf, C. Data Mining the C–C Cross-Coupling Genome. *ChemCatChem* **2019**, *11*, 4096–4107.
- (41) Ceriotti, M.; Tribello, G. A.; Parrinello, M. Simplifying the Representation of Complex Free-Energy Landscapes Using Sketch-Map. *Proc. Natl. Acad. Sci. U. S. A.* **2011**, *108*, 13023–13028.
- (42) Ceriotti, M.; Tribello, G. A.; Parrinello, M. Demonstrating the Transferability and the Descriptive Power of Sketch-Map. *J. Chem. Theory Comput.* **2013**, *9*, 1521–1532.
- (43) Sawatlon, B.; Wodrich, M. D.; Corminboeuf, C. Unraveling Metal/Pincer Ligand Effects in the Catalytic Hydrogenation of Carbon Dioxide to Formate. *Organometallics* **2018**, *37*, 4568–4575.
- (44) Cordova, M.; Wodrich, M. D.; Meyer, B.; Sawatlon, B.; Corminboeuf, C. Data-Driven Advancement of Homogeneous Nickel Catalyst Activity for Aryl Ether Cleavage. *ACS Catal.* **2020**, *10*, 7021–7031.
- (45) Younus, H. A.; Ahmad, N.; Chughtai, A. H.; Vandichel, M.; Busch, M.; Van Hecke, K.; Yusubov, M.; Song, S.; Verpoort, F. A Robust Molecular Catalyst Generated In Situ for Photo- and Electrochemical Water Oxidation. *ChemSusChem* **2017**, *10*, 862–875.
- (46) Craig, M. J.; Coulter, G.; Dolan, E.; Soriano-López, J.; Mates-Torres, E.; Schmitt, W.; García-Melchor, M. Universal Scaling Relations for the Rational Design of Molecular Water Oxidation Catalysts with Near-Zero Overpotential. *Nat. Commun.* **2019**, *10*, 4993.
- (47) Wang, Y.; Montoya, J. H.; Tsai, C.; Ahlquist, M. S. G.; Nørskov, J. K.; Studt, F. Scaling Relationships for Binding Energies of Transition Metal Complexes. *Catal. Lett.* **2016**, *146*, 304–308.
- (48) Anand, M.; Nørskov, J. K. Scaling Relations in Homogeneous Catalysis: Analyzing the Buchwald–Hartwig Amination Reaction. *ACS Catal.* **2020**, *10*, 336–345.
- (49) Sues, P. E.; Lough, A. J.; Morris, R. H. Stereoelectronic Factors in Iron Catalysis: Synthesis and Characterization of Aryl-Substituted Iron(II) Carbonyl P–N–N–P Complexes and Their Use in the Asymmetric Transfer Hydrogenation of Ketones. *Organometallics* **2011**, *30*, 4418–4431.
- (50) Zagal, J. H.; Koper, M. T. M. Reactivity Descriptors for the Activity of Molecular MN<sub>4</sub> Catalysts for the Oxygen Reduction Reaction. *Angew. Chem., Int. Ed.* **2016**, *55*, 14510–14521.
- (51) Pegis, M. L.; Wise, C. F.; Koronkiewicz, B.; Mayer, J. M. Identifying and Breaking Scaling Relations in Molecular Catalysis of Electrochemical Reactions. *J. Am. Chem. Soc.* **2017**, *139*, 11000–11003.
- (52) Gani, T. Z. H.; Kulik, H. J. Understanding and Breaking Scaling Relations in Single-Site Catalysis: Methane to Methanol Conversion by Fe<sup>IV</sup>=O. *ACS Catal.* **2018**, *8*, 975–986.
- (53) Martin, D. J.; Mercado, B. Q.; Mayer, J. M. Combining Scaling Relationships Overcomes Rate versus Overpotential Trade-Offs in O<sub>2</sub>Molecular Electrocatalysis. *Sci. Adv.* **2020**, *6*, eaaz3318.
- (54) Lan, Z.; Mallikarjun Sharada, S. Linear Free Energy Relationships for Transition Metal Chemistry: Case Study of CH Activation with Copper–Oxygen Complexes. *Phys. Chem. Chem. Phys.* **2020**, *22*, 7155–7159.
- (55) Falivene, L.; Kozlov, S. M.; Cavallo, L. Constructing Bridges between Computational Tools in Heterogeneous and Homogeneous Catalysis. *ACS Catal.* **2018**, *8*, 5637–5656.
- (56) Yang, L.-C.; Hong, X. Scaling Relationships and Volcano Plots of Homogeneous Transition Metal Catalysis. *Dalton Trans.* **2020**, *49*, 3652–3657.
- (57) Anand, M.; Rohr, B.; Statt, M. J.; Nørskov, J. K. Scaling Relationships and Volcano Plots in Homogeneous Catalysis. *J. Phys. Chem. Lett.* **2020**, *11*, 8518–8526.
- (58) While our molecular volcanoes are able to predict catalytic activity and selectivity from a single descriptor variable or a handful of descriptor variables, they are currently incapable of probing the lifespan of a catalyst. Thus, at this time we cannot consider all aspects of the catalytic “devil’s triangle”.